Journal of Materials Chemistry C

Functional thin film coatings incorporating gold nanoparticles in a transparent conducting fluorine doped tin oxide matrix

Journal:	*Journal of Materials Chemistry C*
Manuscript ID:	TC-ART-10-2014-002275.R1
Article Type:	Paper
Date Submitted by the Author:	01-Dec-2014

Complete List of Authors:	Chew, Clair; University College London, Chemistry Bishop, Peter; Johnson Matthey Technology Centre, Salcianu, Carman; Johnson Matthey Technology Centre, Carmalt, Claire; University College London, Department of Chemistry Parkin, Ivan; University College London, Department of Chemistry

ARTICLE TYPE www. rsc.org/xxxxxx | XXXXXXXX

Functional thin film coatings incorporating gold nanoparticles in a transparent conducting fluorine doped tin oxide matrix†

Clair K. T. Chew,[a] Carmen Salcianu,[b] Peter Bishop, [b] Claire J. Carmalt,[a] and Ivan P. Parkin[a]*

Received Xth XXXXXXXXXX 20XX, Accepted Xth XXXXXXXXX 20XX
First published on the web Xth XXXXXXXXXX 200X
DOI: 10.1039/b000000x

Noble nanoparticle-metal oxide composites attract research interest due to their unique combination of properties. We report the successful combination of gold nanoparticles (AuNPs) and F-doped SnO_2 making composites by layering, producing films that demonstrate unique and interesting optoelectronic properties - high visible transparency, electrical conductivity and with additional plasmonic effects. Both of the layers were deposited by aerosol assisted chemical vapour deposition (AACVD) onto heated glass substrates. Four distinctive sets of films were prepared and analysed consisting of: gold nanoparticles, F-doped SnO_2 (FTO), a layer of gold nanoparticles on FTO and an FTO layer on gold nanoparticles. The sizes of the AuNPs were shown to depend on the precursor concentration used. Layered Au:FTO composite films have an attractive blue colouration from the surface plasmon resonance (SPR) of the AuNPs yet have high transparency in the visible region and are electrically conducting, comparable to commercial FTO.

1 Introduction

Evidence for the use of nanoparticles colouring glass can be traced back to the 4th or 5th century AD, a famous example being the Lycurgus cup. Production of ruby red glass began in the 17th century with the use of Purple of Cassius - the product of a reaction between gold salts with tin (II) chloride.[1] It was thought that a Au:Sn alloy was the source of the colour, but we now know that the true origin of colour was the Au nanoparticles supported on tin dioxide.[2] Nowadays coloured glass for architectural windows is highly sought after and is traditionally introduced by body tinting via doping with various metal oxides such as cobalt oxide for blue glass.[3] However since the metal oxide dopant is introduced into the liquid part of the flow process of glass production, when changeover is needed large amounts of waste are generated when flushing the system. We propose that a gold nanoparticle coating could be used as a potential colourant for modern glass production.

The colour of gold nanoparticles (AuNPs) originate from strongly localised surface plasmon resonance (SPR), which changes according to the size and shape of the particles and the surrounding dielectric media.[4] This allows the character of the nanoparticles to be fine-tuned using different factors and adjusted for many different applications other than a colourant, such as in sensors, catalysis and imaging.[5] There have been reports that by depositing noble nanoparticles alongside metal oxides, desirable functional optoelectronic properties can be improved: examples are enhanced third-order nonlinear susceptibility,[6] increased photocatalytic conductivity of TiO_2 [7–9] and the improvement of switching properties in a WO_{2-x} electrochromic system.[10] Another important gold:metal oxide application worth a mention is metal oxide supported gold catalysts, whereby the catalytic activity of the gold is related to it's state as a composite with the metal oxide. The extent of this catalytic activity can be related to the other functional properties of AuNP and metal oxide composite.

In this paper we look at the combination of AuNPs and fluorine doped tin dioxide (FTO). The majority of FTO is deposited for low emissivity coatings on architectural glass,[11,12] but it's also used as a transparent electrode in amorphous silicon solar cells and flat panel displays. The various number of applications make FTO an important transparent conducting oxide (TCO) material for solar energy conversion and new optoelectronic devies. TCOs achieve their optical transparency and electronic conductivity by having a conduction band sufficiently populated with charge carriers for electrical conduction yet maintaining a large band gap.[13] The current FTO system have been reported to have a resistivity, on the order of 10^{-4} Ω cm and an optical transparency of over 80 % at 550 nm.[14,15] Two other major considerations in determining the electrical conductivity of TCOs are the electron mobility, μ and charge carrier concentration, n.

Gold nanoparticle:metal oxide matrices have mostly been deposited in bulk form or as thin films,[16,17] they have also been synthesised as nanowires[18] and nanocomposite parti-

[a] *Materials Chemistry Research Centre, Department of Chemistry, 20 Gordon Street, London, WC1H 0AJ, United Kingdom. Fax: XX XXXX XXXX; Tel: XX XXXX XXXX; E-mail: xxxx@aaa.bbb.ccc*
[b] *Johnson Matthey Technology Centre, Blounts Court Road, Sonning Road, Reading, West Berkshire, RG4 9NH, United Kingdom.*

cles.[19] More specifically for Au:SnO_2 composites, powders and nanoparticles have been synthesised for their use as gas sensors.[20–22] Recently a thin film of Au nanoparticles embedded in SnO_2 was spin coated from a sol-gel solution of SnO_2 coated Au nanoparticles to ensure a homogenous film.[23] AACVD experiments have also been used to deposit various AuNPs and metal oxide nanocomposites on glass in a single-step process.[24,25] The deposition procedure is closely related to the industrial way of coating glass and results in composite films with the desired optoelectronic properties, not reported from other methods such as sol gel[23] and sputtering.[16] The focus of this paper are films with high visible transparency, low resistivity, a blue colouration, SPR absorbance and adherence to the glass substrate.

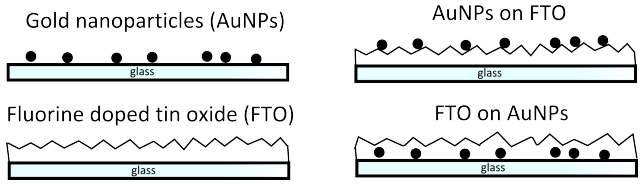

Fig. 1 Schematic of layers deposited.

We showcase the ability of aerosol assisted chemical vapour deposition (AACVD) to efficiently form AuNPs *in-situ* from auric acid. These were deposited onto glass (AuNP/glass) or on top of FTO (AuNP/FTO) (Figure 1). The individual AuNPs and FTO depositions were optimised and subsequently deposited on top of each other, achieving layered composite thin films in a controlled manner. The thin films presented here successfully combine the plasmonic resonance from AuNPs with excellent TCO properties, achieving figures of merit (sheet resistance, charge carrier concentration, mobility) that were equal or better than commercial TCO materials. The layered FTO-gold films maintained the TCO properties whilst also enhancing the visual appearance to give a blue-TCO material. The method used here is a straightforward and versatile way of synthesising and investigating the properties of metal oxide, gold nanoparticulate and composite gold metal oxide films.[26] Because the gold nanoparticles become well adhered to the substrate due to the presence of the metal oxide layer, above or below it, the method is envisaged to be easily inserted into the process of glass coating.

2 Experimental Details

2.1 Materials.

Butyltin trichloride ($SnBuCl_3$) and ammonium fluoride (NH_4F) were purchased from Sigma-Aldrich Chemical Co. Hydrogen tetrachloroaurate (III) hydrate was supplied from Alfa Aeser by Johnson Matthey Plc. Methanol (MeOH) was bought from Fisher Chemical.

2.2 Chemical vapour deoposition.

The films were deposited by aerosol assisted chemical vapour deposition (AACVD) in a cold-walled horizontal-bed CVD reactor. A top and bottom plate was placed in the reactor for depositions to occur on which were composed of SiO_2 barrier glass (dimensions approximately 145 x 45 x 5 mm) supplied by Pilkington NSG. The top plate was positioned 8 mm above and parallel to the bottom plate, the complete assembly inside of a quartz tube. Depositions were carried out on the barrier layer to prevent possible ion transfer from the bulk glass. The reactor was heated using a carbon block positioned under the bottom plate. Aerosols of precursor solutions were generated from a PIFCO-HEALTH ultrasonic humidifier with an operating frequency of 50 kHz and 20 W of power. The aerosol was then carried into the reactor using a flow of air via polytetrafluoroethylene and glass tubing, entering the reactor in between the top and bottom plates. Any waste left the reactor through the exhaust at the other end. The carrier gas transported the aerosol from the flask until all the liquid was used which took around 20-40 mins. All the depositions were carried out at 450 °C and with an air flow of 1 or 2 L min^{-1} for the FTO and gold nanoparticle (AuNPs) films respectively. The thin films of FTO and AuNPs were deposited by themselves (single layered) or one above the other (double layered FTO on AuNPs or AuNPs on FTO). When the depositions were completed the heat and air flow was turned off and the plates left to cool to room temperature. The cooled plates were then removed and handled in air.

2.3 Precursor solutions.

All the precursor compounds were dissolved in methanol. Auric acid ($HAuCl_4.xH_2O$) was used as a precursor for the gold depositions and monobutyltin trichloride ($BuSnCl_3$, MBTC) with ammonium fluoride (NH_4F) for the fluorine doped tin oxide (FTO).

2.4 Characterisation techniques.

Scanning electron microscopy (SEM) was carried out on a JEOL 6301F instrument using voltages between 5 and 20 kV. Energy Dispersive X-ray (EDX) analysis was also carried out on the same instrument at an operating frequency of 20 kV. X-ray Diffraction (XRD) patterns were measured on a Bruker-Axs D8 (GADDS) diffractometer using monochromated Cu K radiation. UV-vis spectra were taken using a Perkin Elmer Fourier Transform Lambda 950 UV-vis spectrophotometer over 190 - 3300 nm. X-ray photoelectron spectroscopy (XPS) elemental analysis was carried out using a

Thermo Scientific K-Alpha. Room temperature Hall effect measurements were carried out on an Ecopia HMS 3000 set up in the Van der Pauw configuration. Measurements were taken with a 0.58 T permanent magnet and a current of 1 μA. Tests were carried out on a 1 x 1 cm sample. Ohmic contacts were established with silver paint (Agar scientific) and tested prior to measuring with the in-built software. Film thickness was measured and taken from a Filmetrics F20 machine operating in reflectance mode in air against an as-supplied FTO standard. Using the film thickness, the Hall effect was used to measure resistivity ρ, mobility μ and charge carrier concentration n.

3 Results and Discussion

3.1 CVD of gold nanoparticles

Films of gold nanoparticles (AuNPs) were deposited by AACVD at 450 °C from precursor solutions of auric acid in methanol at different concentrations (Table 1). The gold depositions occurred consistently on both the top and bottom plates, therefore both plates were analysed in order to understand the reactor chemistry.

Table 1 Precursor solutions used for depositions, all dissolved into 20 ml methanol.

Thin film	Precursor	Amount (mmol)
Gold nanoparticles	$HAuCl_4$	(0.5, 1 and 2) x 10^{-2}
Fluorine doped tin dioxide	MBTC and NH_4F	0.53 and 0.17

The films of Au-nanoparticles were purple and pink in colour, powdery and relatively non-adherent to the glass rubbing off easily with everyday handling, which is expected for glass that has not been pretreated.[29] The AuNP films did not alter when reheated up to 450 °C for 30 minutes in the reactor. All the XRD patterns from depositions using auric acid display crystalline cubic gold. EDX further confirmed the presence of nanoparticle metallic gold corresponding to the bright areas in SEM images. The thin films of AuNPs on glass were imaged under SEM and also delaminated and measured using TEM. SEMs (Figure 2 a and d) of the films show that the gold films were particulate and non-continuous resulting in non-conductive materials. At first glance the particles seem to be spherical, however on closer investigations of the SEM and TEM (Figure 2a, d and 3) images a variety of faceted shapes were also found. In Figure 2 the SEM images and optical absorption can be seen.

3.2 Differences between bottom and top plate gold depositions.

The sizes of the nanoparticles deposited on the top plate were in general slightly larger (30-70 nm) compared to the bottom plate (20-60 nm). The sizes of the NPs correspond to its SPR maxima, with the SPR absorptions of larger top plate nanoparticles located at longer wavelengths compared to the corresponding bottom plate nanoparticles. Even though the nanoparticles on the top plates were larger, fewer nanoparticles were observed as a larger area of glass can be observed from SEM images and XRD patterns. AuNPs are formed when auric acid is reduced by methanol in the reactor where the temperature is high enough for reaction activation, this can occur in between the plates or more often near the heat source i.e. the bottom plate. Larger particles which form in between the plates are more likely to be affected by thermophoresis, a process where larger particles are pushed upwards due to convection in the reactor, in this case eventually settling on the top plate. Since AuNPs form more easily nearer the heated substrate, AuNP formation and deposition is more likely to occur on the bottom plate and we observe a higher concentration of AuNPs on the bottom plate.

3.3 Effect of auric acid precursor concentration.

Nanoparticles were deposited from a range of precursor concentrations (0.5, 1 and 2 x 10^{-2} mmol) which resulted in a range of sizes. Higher concentrations of gold in the precursor solution resulted in larger and more irregular sized particles with a larger dispersity (Figure 3). Similarly to NPs deposited on the top plate, the SPR absorption maxima were observed at longer wavelengths (Table 2). As the concentration of auric acid was lowered the nanoparticles became smaller and more spherically uniform, getting down to 10 nm (see TEM images in Figure 3). This trend was only seen on the bottom plate, all the top plate nanoparticles had a large size variation and were irregularly shaped, however the amount of nanoparticles did decrease in correlation with the auric acid concentration.

Table 2 The different concentrations of auric acid in methanol used to deposit the gold nanoparticles and their corresponding SPR maxima and sizes determined from SEM images.

Amount of $HAuCl_4$ (mmol)	SPR maximum (nm) of bottom plate substrate and top plate (nm)	Range of nanoparticles observed (nm)
0.5 x 10^{-2}	535; 540	10-40
1 x 10^{-2}	540; 560	30-50
2 x 10^{-2}	545; 570	50-70

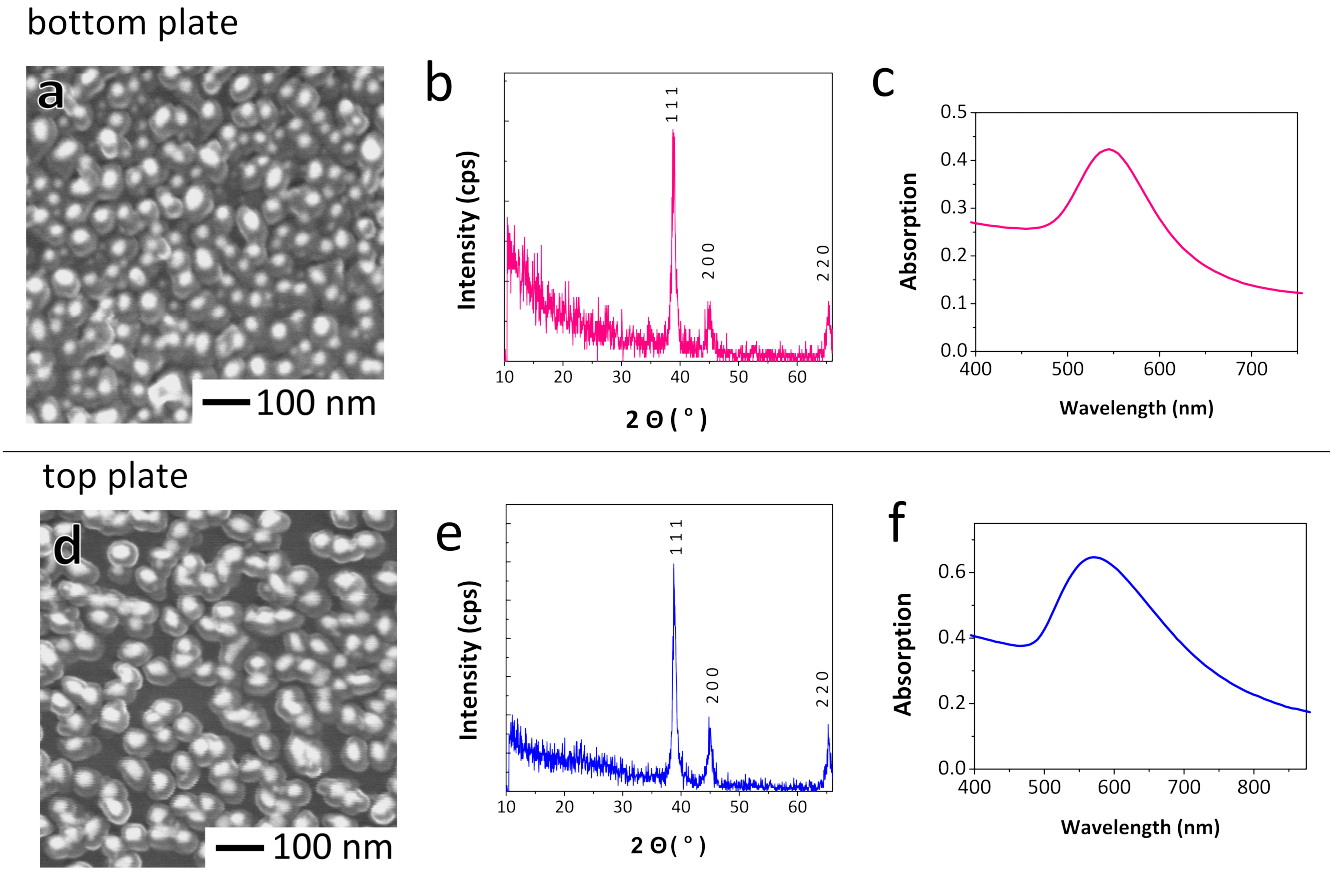

Fig. 2 Comparison of films deposited on bottom and top plate deposited from the AACVD reaction of auric acid (0.02 mmol) in methanol (20 ml) with air (2 Lmin-1) at 450 °C. SEM images of gold nanoparticles deposited on the bottom (a) and top plate (b). The corresponding XRD patterns (c,d) show cubic gold. The SPR maximum can be observed from the absorption spectra at (e) 545 nm and (f) 570 nm.

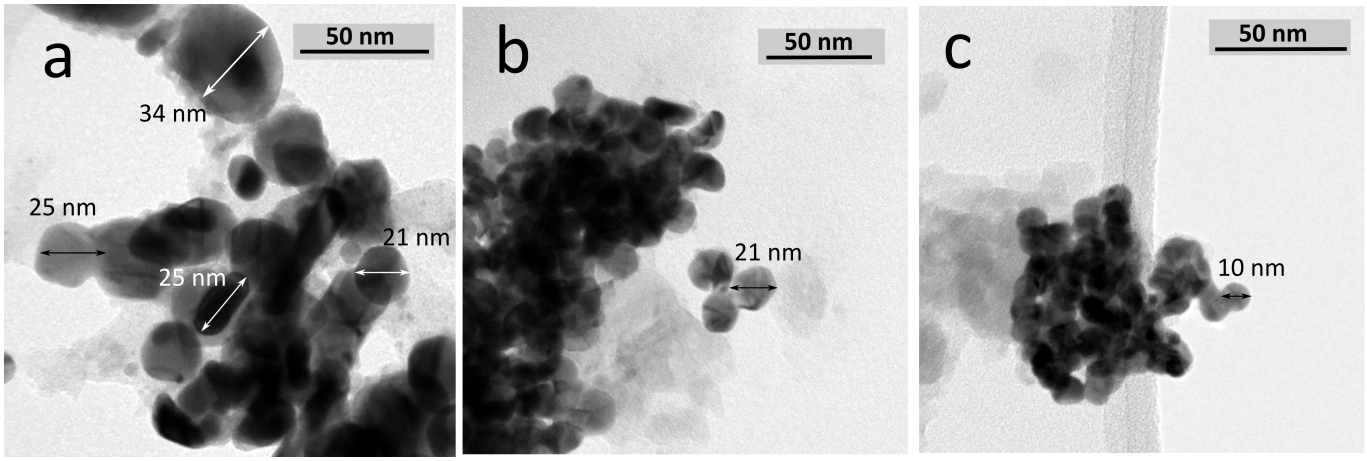

Fig. 3 TEM images of delaminated AuNPs deposited with different concentrations of HAuCl4 (a) 2 x 10^{-2} mmol, (b) 1 x 10^{-2} mmol and (c) 0.5 x 10^{-2} mmol.

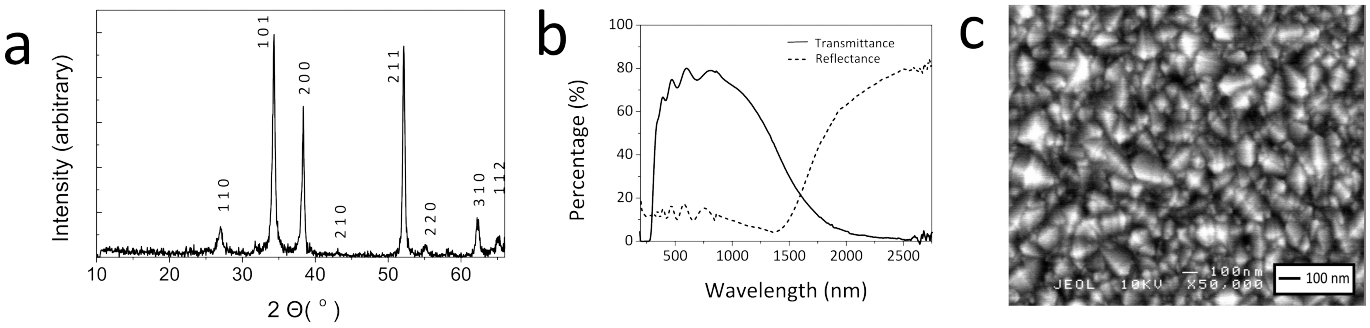

Fig. 4 (a) XRD pattern, (b) transmittance and reflectance spectra and (c) SEM image of FTO deposited by AACVD from a solution of butyltin trichloride and ammonium fluoride at 450 C.

3.4 Properties of fluorine doped tin oxide thin film.

Fluorine doped tin oxide (FTO) was deposited from a 30 % F:Sn precursor solution (NH_4F:$BuSnCl_3$ in methanol) at 450 °C. The FTO thin film (around 500 nm thick) displayed sharp SnO_2 reflections in the XRD patterns with a typical pyramidal microstructure as observed from SEM images (Figure 4 c). Preferred orientation was found in the (200) and (211) planes which correlate with low electrical resistivity agreeing with previous FTO studies.[14] The film adhered well to the glass, passed the Scotch® tape test and could not be rubbed off unless scratched with a metal spatula. The transmittance was high at around 70-80 % in the visible region (see Figure 4b and Figure 6b). Measurements using the Hall effect and Van der Pauw calculations show that the FTO thin film on glass is n-type with a charge carrier concentration of 4.9 x 10^{20} cm^{-3}, mobility 25 cm^2 $(V\ s)^{-1}$, sheet resistance 10 Ω / □ and resistivity 5.0 x 10^{-4} Ω cm. These figures are comparable and in some cases exceed those of the leading commercial TCO for glass Pilkington TEC-8, which has a carrier concentration 5.3 x 10^{20} cm^{-3}, mobility 28 cm^2 $(V\ s)^{-1}$, sheet resistance at 8 Ω / □ and resistivity 5.2 x 10^{-4} Ω cm. The electrical properties are in line with the reflectance spectra which display the characteristic plasma band onset (Figure 4 b) due to high charge carrier concentration and an interference pattern due to the thickness of the film.[27] This long wavelength reflectivity is associated with low emissivity coatings and the FTO presented here possesses a near ideal reflection/transmission profile (Figure 4 b).

3.5 Composite gold nanoparticle and FTO thin films by layering.

The AuNPs and FTO layers were then combined to create double layered thin films of either FTO on AuNPs (FTO/AuNP) or vice versa (AuNP/FTO). The deposition conditions of the layered films were identical to the single layered thin films described above. This allowed optimum deposition conditions to be determined before layering the materials, enabling us to combine the desirable characteristics of the individual films. The layering method allowed us options of either exposing the AuNPs on the material surface, or if the metal oxide surface needs to be exposed placing the AuNPs as the bottom layer. AuNPs are traditionally relatively non-adherent to glass[24] unless complicated methods such as pretreating the glass[28] or silanisation[29] are employed. Using the layering method, the AuNPs were robustly adhered by depositing FTO above it and also surprisingly when formed on top of the FTO suggesting the presence of strong interaction between the gold nanoparticles and semiconducting FTO. All the composite films were adherent, passing the Scotch tape test, with no visible change after months of storage and only scratching off when using a steel scalpel with force.

3.6 Fluorine dope tin dioxide on gold nanoparticles (FTO/AuNP).

For layered films of FTO on AuNPs (FTO/AuNP), a range of AuNPs were deposited first, using the same precursor concentrations as in Table 1, with a subsequent FTO layer made using a F:Sn 30 % precursor solution (NH_4F:$BuSnCl_3$ in methanol). The resulting films were blue and transparent with the FTO acting as a sealant adhering the AuNPs to the glass. Most of the FTO/AuNP films displayed a SnO_2 pattern in the XRD pattern with preferred orientation in the (200) and (210) plane (Figure 5 a and d) the same as FTO deposited onto glass. An exception was found for the layered films where FTO was deposited on a highly concentrated layer of AuNPs, from the highest auric acid precursor concentration investigated (2 x 10^{-2} mmol of $HAuCl_4$), whereby the preferred orientation was solely (200). The change in preferred orientation is reflected in the broader particle morphology observed from SEM images (Figure 5 c) which could be due to a disturbance in the growth of the film from the shape of the underlying AuNPs.

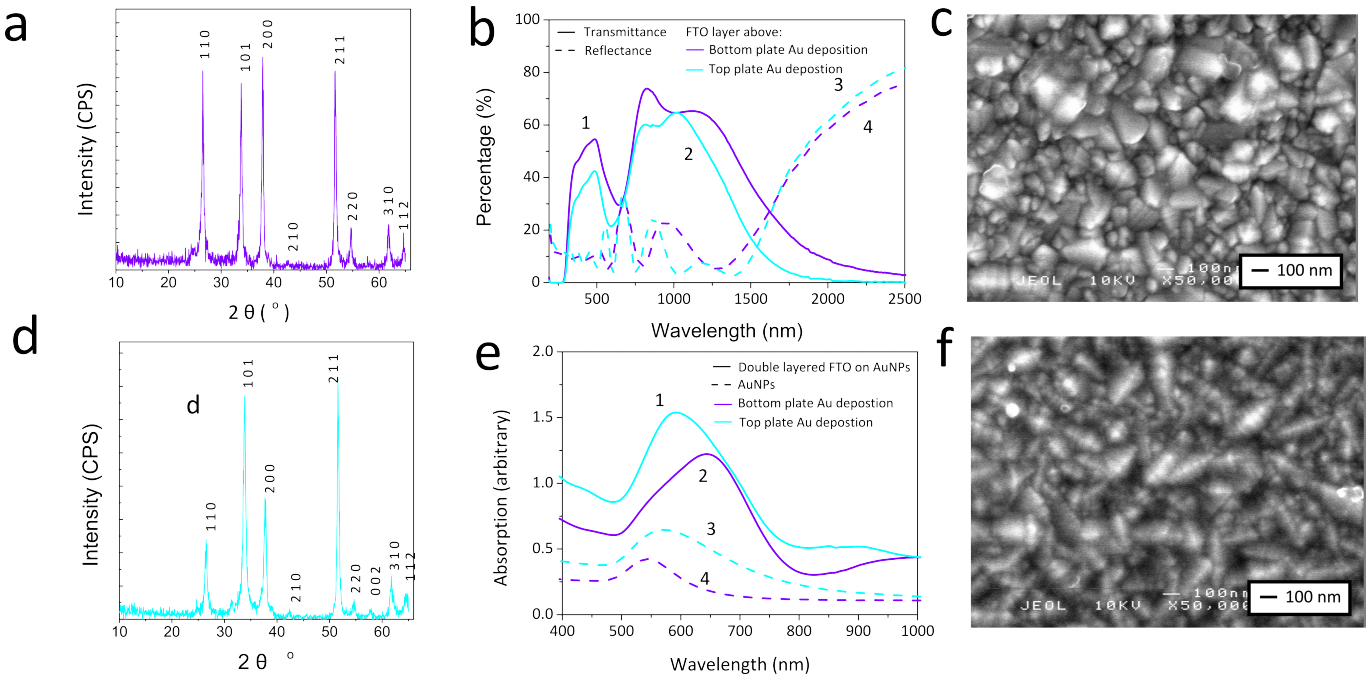

Fig. 5 Comparing the properties of composite FTO (30 % ratio of F:Sn) depositions on AuNP substrates from top and bottom plate positions. XRD patterns of FTO deposited on bottom (a) and top (d) plate AuNPs. The transmittance and reflectance spectra (b) can be seen for FTO deposited on the bottom and top plate of a gold nanoparticle deposition. The corresponding SPR of AuNPs (e) can be seen to shift to longer wavelengths FTO layer deposition. Different morphologies were observed from the SEM images of FTO on bottom plate (c) and top plate (f).

Table 3 Electronic properties of FTO on AuNPs layered thin film. Precursor solutions were composed of 30 % F:Sn for FTO and 2 x 10^{-2} mmol HAuCl(x 10^{-4} Ω cm for AuNPs.

Substrate for FTO deposition	ρ, resistivity (x 10^{-4} Ω cm)	R_{SH}, sheet resistance (sq^{-1})	μ, mobility ($cm^2(Vs)^{-1}$)	N, carrier concentration (cm^{-3})
Glass	5	10	25.3	4.93 x 10^{20}
AuNPs (top plate)	-	-	28.44	4.26 x 10^{20}
AuNPs (bottom plate)	4.86	7.84	25.73	4.99 x 10^{20}

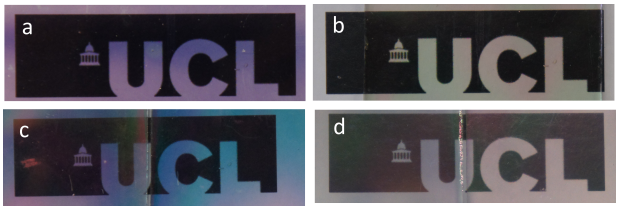

Fig. 6 Photographs of films showing the colour and transparency. (a) AuNPs deposited from auric acid, (b) FTO deposited from MBTC and NH_4F, (c) FTO deposited on top of AuNPs and (d) AuNPs deposited above FTO.

The colour of the films change from pink/purple AuNPs to blue after FTO deposition (Figure 6a and c), indicating that the absorption has moved towards the red end of the spectrum. This correlates with the location of the AuNPs SPR maximum, which generally shifts to longer wavelengths after FTO deposition as a consequence of the change in surrounding dielectric constant by having the FTO in-fill the AuNP structure. The transmittance and reflectance plots are simply a combination of the two individual films.

The measured electronic properties (Table 3) of the FTO/AuNPs were retained, with the reflection in the far IR due to the onset of the plasmon band not affected by a AuNP substrate (Figure 5c) when compared to the reflection spectrum of the FTO (Figure 4b) thin film. This could mean that no electron transfer is occurring in between the layers. It should be noted that the blue colouration from the SPR combined with the reflection in the far IR is an ideal one for window applications.

3.7 Gold nanoparticles on fluorine doped tin dioxide (AuNP/FTO).

For AuNPs on FTO layered materials, the FTO was deposited first with a precursor concentration of 30 % F:Sn in methanol. The FTO films were then used as the top and bottom plate in the same auric acid deposition set up as described in the first section using precursor concentrations as in Table 1. The AuNPs seem adhered better to the FTO than the glass suggesting a strong intermolecular interaction between them perhaps due to the fact that FTO is semiconducting whilst the silica on glass is insulating. As expected with FTO being deposited on glass, the preferred orientation was found to be in the SnO_2 (200) and (210) planes. A small peak at around $2\theta = 45°$ is attributed to the cubic gold (200) plane which was not observed in the XRD pattern of the FTO overlaid on AuNPs layered film.

Only the films deposited with a high auric acid concentration (2 x 10^{-2} mmol) have small but detectable SPR absorption maxima at 528 and 562 nm for bottom and top plate films respectively (arrows Figure 7). Despite the lack of visible SPR, all the films still have a lighter pink purple colouration indicating that there was indeed a layer of AuNPs (Figure 6). The position of the visible SPR maxima follows the trend of previous films whereby the position of the bottom plate AuNPs maximum is at a shorter wavelength compared to the top plate AuNP film, again indicating that top plate depositions result in larger AuNPs. When comparing the detectable SPR maxima of AuNP/FTO and AuNP/glass, a slight shift to lower wavelengths was observed. This is a combination of the dielectric character of the FTO as well as different substrate conditions for AuNP formation and deposition.

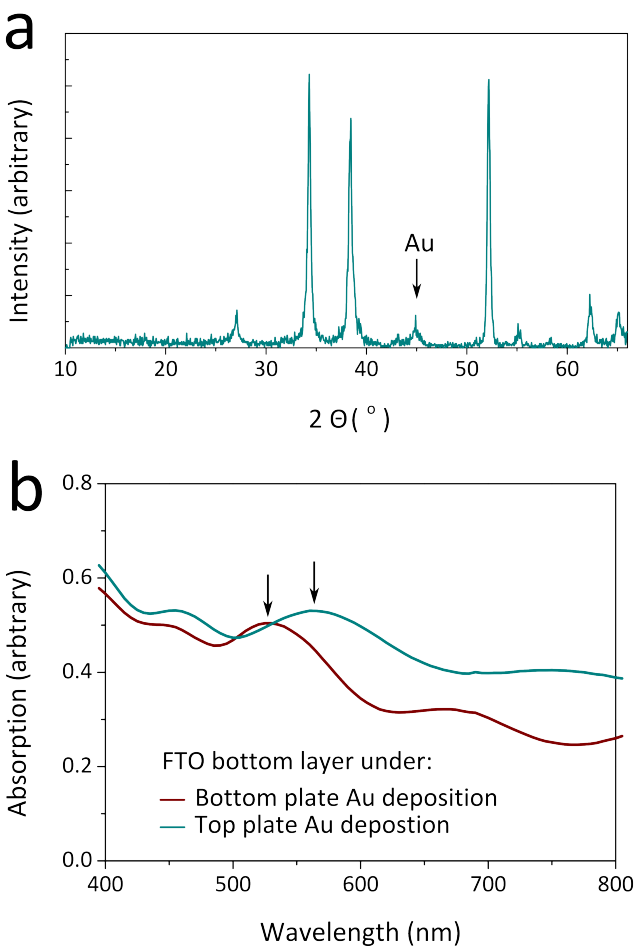

Fig. 7 XRD and optical spectra of AuNPs deposited onto fluorine doped tin oxide thin film. XRD pattern is standard for all the FTO on AuNPs thin film (a). The SPR absorption (arrows) of FTO deposited onto top and bottom plate gold nanoparticles (b).

The deposition of AuNPs nanoparticles on the FTO varied from a very dense layer of spherical NPs to a decorative type shown in Figure 8, at lower auric acid concentration. However, the sizes of the nanoparticles do not seem to vary and

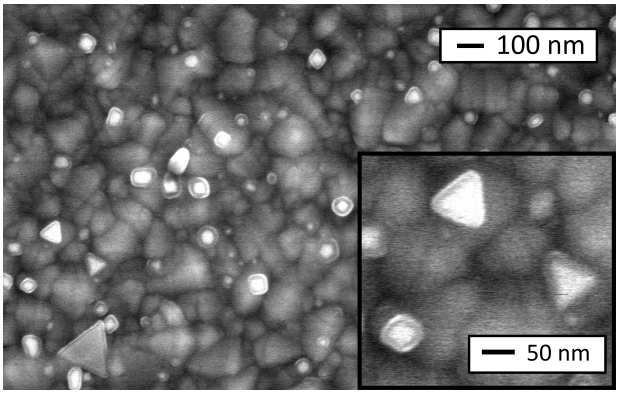

Fig. 8 SEM image of AuNPs (from 0.5 x 10^{-2} mmol auric acid) deposited onto a bottom plate of FTO.

ranged from 30 to 70 nm. AuNPs can be observed in the SEM image even where the SPR was not easily detectable. In general the electronic properties of the AuNPs on FTO thin films were the same as FTO on glass with the resistivities around 5 x 10^{-4} cm.

4 Conclusions

The SPR properties of AuNPs and TCO properties from FTO have been successfully combined into composite materials and characterised. The composite gold nanoparticle and FTO films were deposited using aerosol assisted chemical vapour deposition in a layered structure. The highly transparent and conducting character of the FTO was not altered even when depositing on top a layer of AuNPs with all the films achieving excellent sheet resistances of between 8-10 sq^{-1}. The layered thin film took on the optical character of both layers, combining the SPR absorption (500-700 nm), blue/pink colouration and reflection (onset at 1500 nm) in the IR due to the charge carrier concentration. The refractive index of the FTO film is higher than air at around 2,[30,31] and this shifts the SPR absorption towards longer wavelengths.[4] Considering the *in-situ* AACVD method for making AuNPs without surfactants, the deposition still managed to produce AuNPs homogenously on the surface at approximately the same sizes as each other which were dependant on precursor concentration. This method is to our knowledge the first report of making layered films of TCO with enhanced colouration properties, and can be further studied in terms of a tunable system with easier deposition of composite Au:metal oxide system without the need for an extra *ex-situ* nanoparticle synthesis step.

5 Acknowledgements

IPP, CJC and CKTC thank the EPSRC and Johnson Matthey for funding and provision of auric acid.

References

1 R. von Wagner, *Manual of Chemical Technology*, D. Appleton & co., 1987, p. 452.
2 R. Zsigmondy, *Justus Liebig's Annalen der Chemie*, 1898, **301**, 361–387.
3 J. D. Ruye, *Manufacture of tinted glass*, 1982.
4 S. Underwood and P. Mulvaney, *Langmuir*, 1994, **10**, 3427–3430.
5 C. Chen and E. Burstein, *Physical Review Letters*, 1980, **45**, 1287–1291.
6 H. B. Liao, R. F. Xiao, J. S. Fu, P. Yu, G. K. L. Wong and P. Sheng, *Applied Physics Letters*, 1997, **70**, 1.
7 A. Primo, A. Corma and H. García, *Physical Chemistry Chemical Physics*, 2011, **13**, 886–910.
8 C. Gomes Silva, R. Juárez, T. Marino, R. Molinari and H. García, *Journal of the American Chemical Society*, 2011, **133**, 595–602.
9 Z. Liu, W. Hou, P. Pavaskar, M. Aykol and S. B. Cronin, *Nano Letters*, 2011, **11**, 1111–6.
10 J. Deng, M. Gu and J. Di, *Applied Surface Science*, 2011, **257**, 5903–5907.
11 T. Minami, *Semiconductor Science and Technology*, 2005, **20**, S35–S44.
12 C. G. Granqvist, *Solar Energy Materials and Solar Cells*, 2007, **91**, 1529–1598.
13 Z. M. Jarzebski, *Journal of The Electrochemical Society*, 1976, **123**, 199C.
14 N. Noor and I. P. Parkin, *Journal of Materials Chemistry C*, 2013, **1**, 984.
15 C. Klç and A. Zunger, *Physical Review Letters*, 2002, **88**, 7–10.
16 S. Cho, S. Lee, S.-g. Oh, S. J. Park, W. M. Kim, B.-k. Cheong, M. Chung, K. B. Song, T. S. Lee and S. G. Kim, *Thin Solid Films*, 2000, **377-378**, 97–102.
17 G. Walters and I. P. Parkin, *Journal of Materials Chemistry*, 2009, **19**, 574.
18 M. S. Hu, H. L. Chen, C. H. Shen, L. S. Hong, B. R. Huang, K. H. Chen and L. C. Chen, *Nature materials*, 2006, **5**, 102–6.
19 T. Ung, L. M. Liz-Marzán and P. Mulvaney, *The Journal of Physical Chemistry B*, 2001, **105**, 3441–3452.
20 J. Zhang, X. Liu, S. Wu, M. Xu, X. Guo and S. Wang, *Journal of Materials Chemistry*, 2010, **20**, 6453.
21 P. Manjula, S. Arunkumar and S. V. Manorama, *Sensors and Actuators B: Chemical*, 2011, **152**, 168–175.
22 T. Miller, S. Bakrania, C. Perez and M. Wooldridge, *Journal of Materials Research*, 2011, **20**, 2977–2987.
23 S. H. Lee, D. M. Hoffman, A. J. Jacobson and T. R. Lee, *Chemistry of Materials*, 2013, **25**, 4697–4702.
24 R. G. Palgrave and I. P. Parkin, *Chemistry of Materials*, 2007, **19**, 4639–4647.
25 R. Binions, C. Piccirillo, R. G. Palgrave and I. P. Parkin, *Chemical Vapor Deposition*, 2008, **14**, 33–39.
26 P. Marchand, I. A. Hassan, I. P. Parkin and C. J. Carmalt, *Dalton Transactions*, 2013, **42**, 9406–22.
27 F. Simonis, M. van der Leij and C. Hoogendoorn, *Solar Energy Materials*, 1979, **1**, 221–231.
28 X. Xu, M. Stevens and M. B. Cortie, *Chemistry of Materials*, 2004, **16**, 2259–2266.
29 O. Seitz, M. M. Chehimi, E. Cabet-Deliry, S. Truong, N. Felidj, C. Perruchot, S. J. Greaves and J. F. Watts, *Colloids and Surfaces A: Physicochemical and Engineering Aspects*, 2003, **218**, 225–239.

30 C. F. Wan, R. D. McGrath, W. F. Keenan and S. N. Frank, *Journal of The Electrochemical Society*, 1989, **136**, 1459.
31 W. K. Choi, *Journal of Vacuum Science & Technology A: Vacuum, Surfaces, and Films*, 1996, **14**, 359.

Functional thin film coatings - incorporating gold nanoparticles in a transparent conducting fluorine doped tin oxide matrix

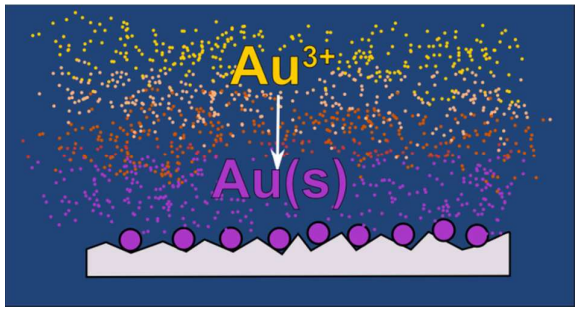

SnO_2 with transparent conducting character have been enhanced with the plasmonic properties of gold nanoparticles using chemical vapour deposition.